



ELSEVIER

Contents lists available at ScienceDirect

Nuclear Instruments and Methods in Physics Research A

journal homepage: www.elsevier.com/locate/nima

Field reconstruction in large aperture quadrupole magnets

A. Lazzaro^{a,1}, F. Cappuzzello^{a,b,*}, A. Cunsolo^{a,b}, M. Cavallaro^{a,b}, A. Foti^{b,c}, S.E.A. Orrigo^a, M.R.D. Rodrigues^a, J.S. Winfield^{a,2}, M. Berz^d

^a INFN-Laboratori Nazionali del Sud, Via S. Sofia 62, I-95125 Catania, Italy

^b Dipartimento di Fisica e Astronomia, Università di Catania, Via S. Sofia 64, I-95125 Catania, Italy

^c INFN-Sezione di Catania, Via S. Sofia 64, I-95125 Catania, Italy

^d Department of Physics and Astronomy, Michigan State University, MI 48824, USA

ARTICLE INFO

Article history:

Received 28 August 2008

Received in revised form

7 January 2009

Accepted 8 January 2009

Available online 19 January 2009

Keywords:

Magnetic spectrometers

Trajectory reconstruction

Field interpolation

ABSTRACT

A technique to interpolate complex three-dimensional field distributions such as those produced by large magnets is presented. It is based on a modified charge density method where the elementary sources of the magnetic field are image charges with Gaussian shape placed on a three-dimensional surface. The strengths of the charges are found as the solution of a best-fit problem, whose special features are discussed in detail. The method is tested against the measured field of the MAGNEX large acceptance quadrupole, showing a high level of accuracy together with an effective compensation of the effect of the experimental errors present in the data. In addition the model field is in general analytical and Maxwellian. As a consequence, the reliability of the presented technique to the challenging problem of trajectory reconstruction in modern large acceptance spectrometers is demonstrated.

© 2009 Elsevier B.V. All rights reserved.

1. Introduction

For magnetic spectrographs with large aperture and energy acceptance, the correction of all the relevant aberrations requires the application of sophisticated techniques based on the reconstruction of the ion trajectories [1,2]. The MAGNEX spectrometer is such an instrument, designed with a solid angle as large as 50 msr and an energy acceptance of $\pm 20\%$, still allowing for an energy, mass and angular resolution as high as 1/1000, 1/250 and 5 mrad, respectively [3–5]. Because of the large accepted phase space, the aberrations are found to be relevant up to high order (10th or so) and could severely limit the design resolutions [6]. To prevent this, the transfer maps need to be computed at least to the same order of the relevant aberrations, which in turn relies on the precise description of the three-dimensional field of each optical element of the spectrograph. This puts severe constraints both on the required accuracy of the field measurement and in the subsequent construction of a field model, based on the interpolation of such data. For example, in Refs. [6–9] it has been shown that in the case of the MAGNEX dipole and quadrupole magnets the standard interpolating methods based on the high order differentiation of the field measured on the

symmetry plane, are not sufficiently accurate to preserve the energy resolution. That is mainly a consequence of the large aperture of these lenses, which amplifies the effect of the experimental errors in the measured field on the high order derivatives necessary for the extrapolation out of the median plane.

In Ref. [9] the problem of the finite uncertainty in the measurement of the magnetic field was analysed for the special case of the MAGNEX quadrupole. It was found that the field data slightly deviate from the ideal axial symmetry, defined in terms of the mechanical shape of the lens, either due to imperfection on the magnetic circuitry or to the finite precision of the alignment of the measurement device. In addition, the two sources of uncertainty were disentangled and the systematic and random errors were estimated. In particular, the systematic errors in the B_x , B_y and B_z components are found to be about 0.3%, 0.2% and 0.05%, respectively, to be compared with the 0.1% approximate limit on the overall field model required for a best application of the trajectory reconstruction technique, such as that based on Differential Algebra (DA) approach [10]. Also the random errors in the B_x , B_y and B_z components are about 0.2%, 0.1% and 0.0%, respectively, which is not negligible. Such errors could rapidly propagate in the interpolation, resulting in much larger figures in the final accuracy of the model field, as happens with standard algorithms based on extrapolation from the median plane. One expects to improve the reliability of the field dataset for the purpose of DA techniques by a proper transformation of the data to account for the systematic errors. Also it is important to use an interpolation algorithm weakly dependent on the random noise at least at the level of 0.2%.

* Corresponding author at: INFN-Laboratori Nazionali del Sud, Via S. Sofia 62, I-95125 Catania, Italy. Tel.: +39 95 542 384.

E-mail address: cappuzzello@lns.infn.it (F. Cappuzzello).

¹ Present address: ST Microelectronics Stradale Primosole, 50 I-95121 Catania, Italy.

² Present address: GSI, Planckstr. 1, 64291 Darmstadt, Germany.

An interesting possibility to face this problem is offered by methods based on the charge density technique [11], such as the Image Magnetic Charge Method (IMCM) [12], where the field is generated by a superposition of Gaussian charge distributions. In principle, this method can be applied for every magnetic lens and the resulting distribution is Maxwellian and infinitely differentiable. This latter feature is desirable if one wants to apply techniques based on DA to obtain the transfer map of ray-tracing spectrometers [13–15]. In addition, one can account for measurements out of the symmetry plane of the magnetic elements, thus avoiding the extrapolations mentioned above. The IMCM has been applied to simple cases where analytic solutions are available and has shown a high accuracy (better than 10^{-4}) and an effective compensation of the randomly distributed measurement errors.

Despite these positive results, the technique of Ref. [12] was notably limited for the following reasons:

- (1) The field was interpolated in a small region of the magnet. No performance tests were done for larger field distributions. This last point is crucial for application to large acceptance spectrometers.
- (2) Only the B_y component was calculated on a central portion of the magnet mid-plane. For applications with real magnets the method should be extended to account for the full \vec{B} vector in the three-dimensional space spanned by the beam envelope.
- (3) The stability of the method against the experimental errors was studied only for the random ones. These latter do not modify the Maxwellian structure of the analytic field, at least in average. For real cases the systematic errors, as for instance those deriving from the misplacement of the measurement device, strongly influence the Maxwellian property. A similar effect is produced by the possible deviations of the field from the expected geometrical symmetry, because of the unavoidable mechanical imperfections of the magnets. The weakening of the Maxwellian property of the measured field could seriously disturb the numerical stability of the IMCM algorithm.
- (4) The behaviour of numerical errors in the boundary regions was not evaluated. For large acceptance spectrometers the correct description of the boundary regions is quite important due to the extended overlap between the beam envelopes and the boundary fields.

The necessary upgrading of the IMCM to account for experimental 3D field distributions could require a big number of image charges and consequently an extraordinary computational effort.

In this paper we show that the number of charges n_c can be greatly reduced by a careful shaping (which is lens dependent) of the grid where they are placed. In this way the error propagation due to the finite numerical precision of the computer drops to an acceptable level. The computational requirements become compatible even with current standard PC capabilities, enabling one to perform challenging tasks such as iterative optimizations of the geometrical parameters of the grid. Thus it is possible to overcome the limitations of the IMCM mentioned above and finally apply it to model real field distributions. We describe a particular version of the IMCM applied to the MAGNEX quadrupole and discuss the compatibility with the severe requirement of the ray reconstruction for this case.

2. Image magnetic charge method: basic concepts

In the original formulation of IMCM the magnetic field of a rectangular iron bar is generated by a superposition of charge distributions of Gaussian shape placed on the nodes of two planar

grids. The strength of each single charge is determined by a least square fit of the field values calculated analytically. In order to reduce any fine structure due to the local influence of each single charge, extended three-dimensional Gaussian distributions of the form [12,14]

$$\rho(r) = \rho_0 \exp\left(-\frac{r^2}{a^2}\right) \quad (1)$$

are used. Here a and ρ_0 are the width and the strength of each individual charge, respectively.

An important complication when applying the method to the MAGNEX quadrupole is represented by the large size of the lens, whose radius is 20 cm and effective length is 58 cm, and the requested accuracy of about 10^{-3} in the reconstructed field. In addition, the number of measured field points is about 10^4 which are almost entirely concentrated in a sector of the magnet. The average error is of the order of 10^{-3} , which is about one order of magnitude more than that studied in Ref. [12]. These factors make n_c easily of the order of 10^4 for an appropriate interpolation of the field distribution. Finally, the measured field slightly deviates from the ideal four-fold symmetry, with the consequence of loss of accuracy if a symmetric charge distribution is used. Alternatively, renouncing the symmetry in the charge distribution, one should increase the number of charges and thus the complexity of the problem. Thus a considerable computational effort would be necessary for a direct application of IMCM to this case, with the consequence of enhancing the numerical error propagation.

In the following a generalization of this method, describing the three-dimensional structure of each component of the magnetic field, is presented.

According to the Gauss law for the rotationally symmetric charge distribution, the i th charge centred at (x_i, y_i, z_i) gives a contribution to the magnetic field at (x, y, z) of the form

$$\begin{aligned} B_{x,i}^C(x, y, z) &= \rho_i \cdot (x - x_i) \cdot F(r_i) \\ B_{y,i}^C(x, y, z) &= \rho_i \cdot (y - y_i) \cdot F(r_i) \\ B_{z,i}^C(x, y, z) &= \rho_i \cdot (z - z_i) \cdot F(r_i) \end{aligned} \quad (2)$$

$$F(r_i) = \frac{1}{r_i^3} \left[-\frac{a_i^2 r_i}{2} \exp\left[-\left(\frac{r_i}{a_i}\right)^2\right] + \frac{a_i^3 \sqrt{\pi}}{4} \operatorname{erf}\left(\frac{r_i}{a_i}\right) \right] \quad (3)$$

where $r_i = [(x - x_i)^2 + (y - y_i)^2 + (z - z_i)^2]^{1/2}$ and $\operatorname{erf}(u) = 2/\sqrt{\pi} \int_0^u e^{-t^2} dt$ is the error function, similarly to Refs. [12–14]. The total field $\vec{B}^C(x, y, z)$ is given by the sum over all the charges. It has been shown that if one tunes appropriately the width parameter, the superposition of regularly distributed Gaussian functions leads to a smooth global distribution [12].

The least square algorithm to determine the charge strengths ρ_i results in a square matrix that must be inverted. If we assume mid-plane symmetry, only one half of these strengths have to be calculated. Since the best-fit matrix A is symmetric the number, N , of independent elements a_{ij} to be calculated is given by

$$N = \frac{n_c(n_c + 1)}{2}. \quad (4)$$

To show how the coefficients of the best-fit matrix are calculated, we rewrite the field components B_x, B_y, B_z as B_1, B_2, B_3 ; then n_1, n_2, n_3 are the numbers of explored points for the B_1, B_2, B_3 components, respectively, and $B_{ij}, i = 1, 2, 3; j = 1, \dots, n_i$, are the individual measured values of the field at the points $(x_{ij}, y_{ij}, z_{ij}), i = 1, 2, 3, j = 1, \dots, n_i$. Finally (x_k^c, y_k^c, z_k^c) are the coordinates of the k th charge placed in the grid above the mid-plane and r_{ijk} the distance between the two points (x_{ij}, y_{ij}, z_{ij}) and (x_k^c, y_k^c, z_k^c) . The strengths of the image charges are obtained by the

solution of the symmetric linear system:

$$A \cdot \vec{\rho} = \vec{b} \Rightarrow \begin{pmatrix} a_{11} & a_{12} & a_{13} & \dots & a_{1n_c} \\ a_{21} & a_{22} & a_{23} & \dots & a_{2n_c} \\ \dots & \dots & \dots & \dots & \dots \\ \dots & \dots & \dots & \dots & \dots \\ a_{n_c1} & a_{n_c2} & a_{n_c3} & \dots & a_{n_cn_c} \end{pmatrix} \cdot \begin{pmatrix} \rho_1 \\ \rho_2 \\ \rho_3 \\ \dots \\ \rho_{n_c} \end{pmatrix} = \begin{pmatrix} b_1 \\ b_2 \\ b_3 \\ \dots \\ b_{n_c} \end{pmatrix}, \quad a_{lm} = a_{ml} \quad (5)$$

where

$$a_{lm} = \sum_{i=1}^{n_1} [(x_{1i} - x_i^c) \cdot F(r_{1il}) - (x_{1i} - x_i^c) \cdot F(\bar{r}_{1il})] \\ \times [(x_{1i} - x_m^c) \cdot F(r_{1im}) - (x_{1i} - x_m^c) \cdot F(\bar{r}_{1im})] \\ + \sum_{i=1}^{n_2} [(y_{2i} - y_i^c) \cdot F(r_{2il}) - (y_{2i} - y_i^c) \cdot F(\bar{r}_{2il})] \\ \times [(y_{2i} - y_m^c) \cdot F(r_{2im}) - (y_{2i} - y_m^c) \cdot F(\bar{r}_{2im})] \\ + \sum_{i=1}^{n_3} [(z_{3i} - z_i^c) \cdot F(r_{3il}) - (z_{3i} - z_i^c) \cdot F(\bar{r}_{3il})] \\ \times [(z_{3i} - z_m^c) \cdot F(r_{3im}) - (z_{3i} - z_m^c) \cdot F(\bar{r}_{3im})] \quad (6)$$

$$b_l = \sum_{i=1}^{n_1} [(x_{1i} - x_i^c) \cdot F(r_{1il}) - (x_{1i} - x_i^c) \cdot F(\bar{r}_{1il})] \\ + \sum_{i=1}^{n_2} [(y_{2i} - y_i^c) \cdot F(r_{2il}) - (y_{2i} - y_i^c) \cdot F(\bar{r}_{2il})] \\ + \sum_{i=1}^{n_3} [(z_{3i} - z_i^c) \cdot F(r_{3il}) - (z_{3i} - z_i^c) \cdot F(\bar{r}_{3il})] \quad (7)$$

In these equations \bar{r}_{ijk} refers to the charge placed below the mid-plane along the same vertical line of the k th one. From Eqs. (6) and (7), it can be shown that the number of calls to the function $F(r_{ijk})$ to calculate all the coefficients of the system in Eq. (5) is

$$(n_1 + n_2 + n_3)[n_c(n_c + 2)] \approx (n_1 + n_2 + n_3)n_c^2 \quad (8)$$

For large field distributions, as in the case of the MAGNEX magnets, n_c could be as high as 10^4 whereas the total number of measured point could easily be of the order of 10^5 . As a consequence the number of function evaluations is approximately 10^{13} . Some computational effort may be saved by using a Chebyshev approximation [16] of the standard error function $erf(x)$ contained in Eq. (3).

3. On the solution of least squares problems with large matrix

One of the main problems in applying the IMCM to the MAGNEX quadrupole is the treatment of the large best-fit matrix. An efficient algorithm guaranteeing a strong numerical stability, high precision and velocity is needed to find the solution of the system of Eq. (5). Different numerical methods were compared [16] to find the best compromise between computational speed and precision:

- (1) Gauss (pivoting);
- (2) Jacobi;
- (3) Gauss–Seidel;

- (4) Cholesky decomposition;
- (5) LU-factorization.

The first method is particularly indicated when small matrices need to be inverted. The matrix $[A]$ is transformed by elementary operations, such as linear combinations of rows or interchange of rows, to a triangular matrix whose solution can be easily found. The number of arithmetic operations required for this is N^3 . As a consequence, for large matrices with dimension $N \geq 100$, the algorithm takes a long calculation time and the finite machine precision strongly affects the solution. Since the best-fit matrix may wander from its symmetry at each step, a large quantity of memory machine is needed to store its N^2 elements in double precision arithmetic.

The Jacobi and Gauss–Seidel methods are iterative and the convergence to the exact solution is ensured only for dominant diagonal or positive definite matrices [16]. They are commonly applied to sparse linear system with most of the matrix elements vanishing. In that case, the convergence from an approximated solution to the exact one is achieved with a few iterations. However, in the case discussed in this paper, the convergence requires more than 10^6 iterations. Moreover, the convergence is not always obtained.

The Cholesky decomposition method requires only $N^3/6$ operations to decompose the best-fit matrix in the product form:

$$A = L \cdot L^T \quad (9)$$

where L is a lower triangular matrix with positive diagonal elements. In this case, only two diagonal systems must be solved whose solution can be found even with simple substitutions. This technique appears quite interesting since it is fast and requires a limited computational effort, at least compared to the others discussed above. A sufficient condition for the Cholesky decomposition is that the matrix A must be positive definite. In our case, this property was achieved up to $N \sim 100$, but an attempt to decompose the A matrix for larger N failed.

In the LU factorization method the matrix A is represented as the product of two matrices,

$$A = L \cdot U \Rightarrow \begin{pmatrix} a_{11} & a_{12} & a_{13} & \dots & a_{1nN} \\ a_{21} & a_{22} & a_{23} & \dots & a_{2N} \\ \dots & \dots & \dots & \dots & \dots \\ \dots & \dots & \dots & \dots & \dots \\ a_{N1} & a_{N2} & a_{N3} & \dots & a_{NN} \end{pmatrix} = \begin{pmatrix} \alpha_{11} & 0 & 0 & \dots & 0 \\ \alpha_{21} & \alpha_{22} & 0 & \dots & 0 \\ \alpha_{31} & \alpha_{32} & \alpha_{33} & \dots & 0 \\ \dots & \dots & \dots & \dots & \dots \\ \alpha_{N1} & \alpha_{N2} & \alpha_{N3} & \dots & \alpha_{NN} \end{pmatrix} \times \begin{pmatrix} \beta_{11} & \beta_{12} & \beta_{13} & \dots & \beta_{1N} \\ 0 & \beta_{22} & \beta_{23} & \dots & \beta_{2N} \\ \dots & \dots & \dots & \dots & \dots \\ \dots & \dots & \dots & \dots & \dots \\ 0 & 0 & 0 & \dots & \beta_{NN} \end{pmatrix} \quad (10)$$

where L is lower triangular and U is upper triangular. In this way the $A \cdot \vec{\rho} = \vec{b}$ equation is transformed as follows:

$$A \cdot \vec{\rho} = (L \cdot U) \cdot \vec{\rho} = L \cdot (U \cdot \vec{\rho}) = \vec{b}. \quad (11)$$

This latter can be solved first for the vector \vec{y} :

$$L \cdot \vec{y} = \vec{b} \quad (12)$$

and then for the vector $\vec{\rho}$:

$$U \cdot \vec{\rho} = \vec{y}. \quad (13)$$

The advantage of this decomposition is that the solution of a triangular set of equations is quite simple. As an example, Eq. (12) can be solved by forward substitution as follows:

$$y_1 = \frac{b_1}{\alpha_{11}}$$

$$y_i = \frac{1}{\alpha_{ii}} \left[b_i - \sum_{j=1}^{i-1} \alpha_{ij} \cdot y_j \right], \quad i = 2, 3, \dots, N \quad (14)$$

while Eq. (13) can then be solved by backward substitution as follows:

$$\rho_N = \frac{y_N}{\beta_{NN}}$$

$$\rho_i = \frac{1}{\beta_{ii}} \left[y_i - \sum_{j=i+1}^N \beta_{ij} \cdot \rho_j \right], \quad i = N-2, N-3, \dots, 1 \quad (15)$$

Eqs. (14) and (15) require, for each element b_i , N^2 executions of a loop containing one multiplication and one addition. In the overall problem of the matrix inversion, one has N elements b_i in the vector. Taking also into account the leading zeros it can be shown that the total number of elementary computations of Eq. (12) is reduced from $N^3/2$ to $N^3/6$, while Eq. (13) is unchanged at $N^3/2$.

The matrix Eq. (11) is thus equivalent to a set of N^2+N linear equations for the α and the β coefficients. An elegant procedure called *CROUT's algorithm* solves this problem [16], merely by arranging them in a special order. Inside this algorithm each a_{ij} is used only once and never again. This means that the corresponding a_{ij} and β_{ij} can be stored in the location before occupied by a_{ij} , which means that the decomposition is “in place”.

In a set of preliminary calculations the precision and the computation time of all the methods summarized above were tested. The LU-decomposition was the best, since the other methods either produced a wrong solution when the number of unknowns become higher than $N \sim 100$ or were by far too slow. LU-decomposition assures good precision and requires small computation time, thus it was used for the application of the IMCM to the MAGNEX quadrupole.

4. IMCM model of the MAGNEX quadrupole

In order to apply the IMCM model to the case of the MAGNEX quadrupole, a special procedure has been set up which performs the following operations:

- (1) Calculates the coefficients of the best-fit matrix, assuming the field symmetries both in the vertical and the horizontal direction and using the Chebyshev approximation for the $\text{erf}(x)$ of Eq. (3). Because of the many calls to this function a reduction of about 20% in the overall computation time was achieved with negligible influence on the final precision.
- (2) Solves the best fit system using a fast and high precision algorithm based on the LU-pivot decomposition method.
- (3) Makes a statistical analysis of the reconstructed field, comparing at each point the discrepancy ΔB_i between the measured and the interpolated fields. In particular, the accuracy of the

reconstructed field, defined by the following quantities:

$$\text{mean absolute error (m.a.e.)} = \frac{\langle |\Delta B_i| \rangle}{B_0} \times 100, \quad i = x, y, z \quad (16)$$

$$\text{mean square error (m.s.e.)} = \frac{\sqrt{\langle (\Delta B_i)^2 \rangle}}{B_0} \times 100, \quad i = x, y, z \quad (17)$$

is estimated.

It was found that the number n_c can be significantly reduced if the charges stay on a series of four cylindrical surfaces, each one with axis parallel to the quadrupole one, thus maintaining the axial symmetry of the mechanical poles. This configuration is shown in Fig. 1, where one of these surfaces is plotted. The angular aperture of the grid was 90° , thus representing a quarter of a cylinder. Only 326 charges, placed at the nodes of such grid, were enough to get an encouraging accuracy to start the optimization. The strength of the charges placed in the other three grids was obtained by the requirement of symmetry both in the horizontal and vertical direction.

Because of the reduced overall computational effort, a series of iterative optimizations can be executed in a reasonable time, giving a better geometric parameterization of the grid. In particular, the tip radius R_1 , the quadrupole radius R_2 and the length L were optimized in such a way. In Table 1 both the quadrupole geometrical parameters and the optimized ones for the charges grid are listed. The field data were supplied in twelve planar grids as reported in Table 2. The actual beam envelope volume covers the planes up to the 7th one. Nevertheless, the full set of data was used, up to the 12th plane, in order to improve the description at the borders of the beam envelope region. Following the technique of the generalized Enge function of Refs. [8,9], supplemental data were added to the measured ones 60 cm beyond the entrance and exit boundaries (i.e., where the measurements end) in order to improve the description of the fringe field of the magnet. The measured value of the field (B_0) at the pole-tip was 0.6 T.

Before comparing the reconstructed field with the experimental data, the influence of possible local fluctuations, such as those generated by random errors in the measurements, on the

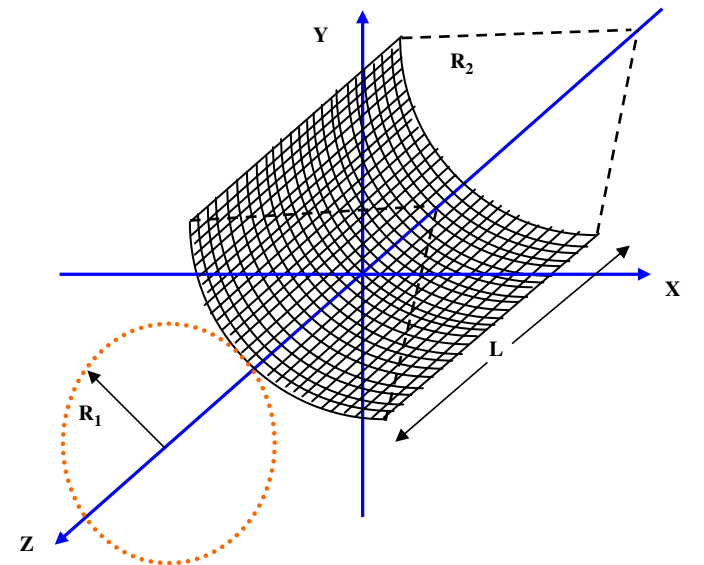


Fig. 1. Geometrical shape of the grid containing the image charges at each node.

overall accuracy was studied. In particular the Maxwellian field generated by the 326 image charges was used to produce virtual data at each point where the actual measurements were performed. Such a field was interpolated by the IMCM technique and the newly calculated data compared with the initial Maxwellian field. In these conditions, which would correspond

Table 1
Geometrical parameters of the quadrupole together with the those of the charges grid.

Quadrupole tip radius	0.2 m	Grid tip radius (R_1)	0.39 m
		Grid curvature radius (R_2)	0.2145 m
Quadrupole length	0.6 m	Grid length (L)	0.6 m
		Grid angular aperture	90°

Table 2
Total number of measured points in the quadrupole mapping for each plane of measurement.

Plane	y (cm)	Number of measured points	x_{min} (cm)	x_{max} (cm)
1	0	2059	-21	21
2	1.5	852	-16.5	0
3	3.0	852	-16.5	0
4	4.5	852	-16.5	0
5	6.0	781	-15	0
6	7.5	781	-15	0
7	9.0	710	-13.5	0
8	10.5	639	-12	0
9	12.0	568	-10.5	0
10	13.5	497	-9	0
11	15.0	426	-7.5	0
12	16.5	213	-3	0

to the ideal case of a field free of experimental errors, the intrinsic accuracy of the IMCM can be estimated. As seen in Fig. 2, the reconstruction accuracy is within the limits for trajectory reconstruction purposes [9] (m.a.e.<0.1% and m.s.e.<0.1%), showing a slight deterioration for the 1st and the 11th plane. This does not influence the overall energy resolution, as the beam envelope covers the volume up the 7th plane. Moreover, the loss of field accuracy near the mechanical poles (which causes an m.s.e. in the 1st plane beyond the requested limit) does not affect the particle trajectories as these cross such region only beyond the exit boundary of the lens.

Then a random source of fluctuations, simulating casual experimental errors, was added to the analytical field at each explored point. A uniform statistical distribution was chosen and different cases analysed with error amplitude ranging from $\Delta B/B_0 = \pm 1-5\%$, in fact much larger than the actual random errors in the experimental dataset ($\Delta B/B_0$ below 0.2%). Some results are shown in the right panels of Fig. 2, where the error amplitude was set to $\Delta B/B_0 = \pm 3\%$. One observes that the corresponding m.a.e and m.s.e. do not show appreciable variations when compared with those obtained in the case (Δ (m.a.e) $\sim 0\%$ Δ (m.s.e) $\sim 0\%$). Thus the method is shown to be particularly powerful for situations where the field inaccuracy is dominated by random errors.

5. Field reconstruction accuracy

The IMCM model of the MAGNEX quadrupole field was compared with the measured one. The calculated accuracy of the model, defined in Eqs. (16) and (17), is shown in Fig. 3 for each plane covered by experimental data. Both the finite error in the

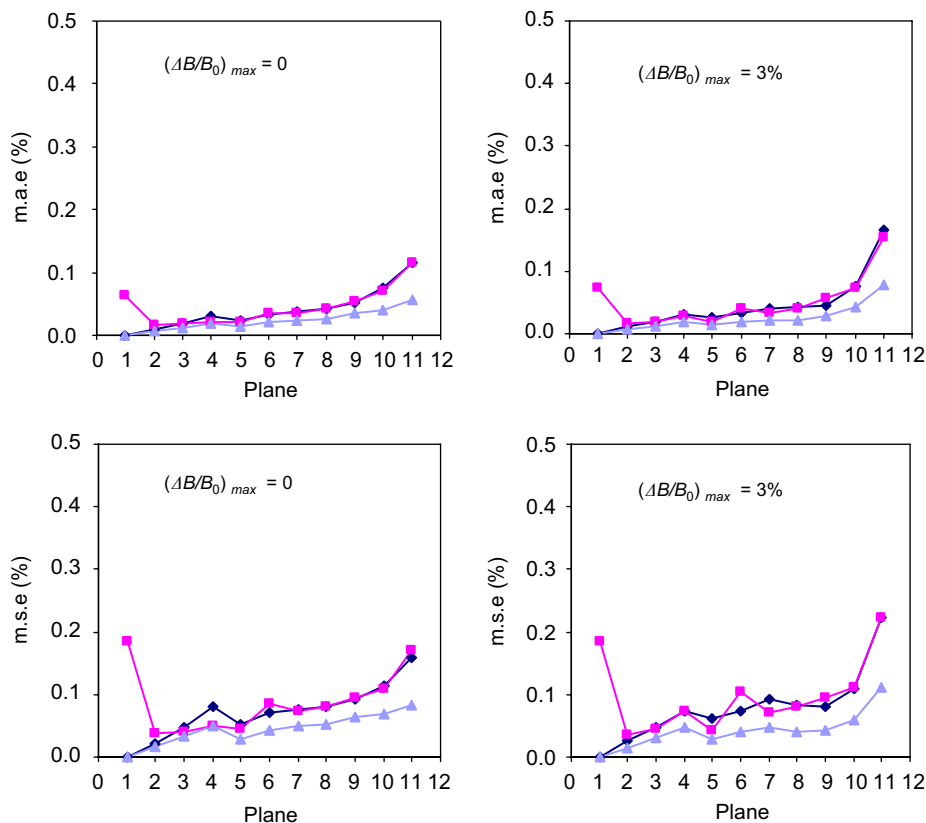


Fig. 2. M.a.e. (upper panels) and m.s.e. (lower panels) as a function of the measurement plane obtained by applying the IMCM method to the analytical quadrupole field. In the right panels, a random and uniform error distribution with $(\Delta B/B_0)_{max} = 3\%$ was added to the analytical field ($B_0 = 0.6$ T, \blacklozenge : B_x ; \blacksquare : B_y ; \blacktriangle : B_z).

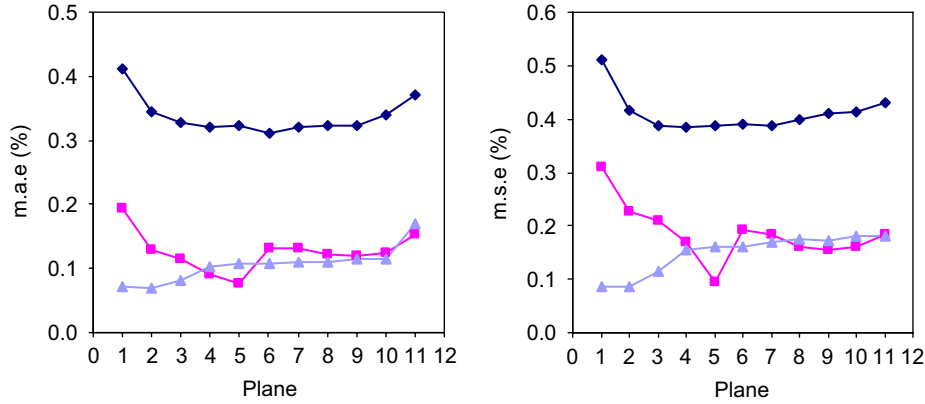


Fig. 3. M.a.e. (left) and m.s.e (right) as a function of the mapping plane obtained by applying the IMCM to the MAGNEX ($B_0 = 0.6\text{ T}$; \blacklozenge : B_x ; \blacksquare : B_y ; \blacktriangle : B_z).

Table 3

Systematic error parameters $\Delta\theta$, $\Delta\varphi$, $\Delta\psi$, $\Delta\theta_p$, $\Delta\varphi_p$, $\Delta\psi_p$ obtained for the quadrupole [9].

Error parameters	Optimized value (deg)
$\Delta\theta$	0.1
$\Delta\varphi$	-0.7
$\Delta\psi$	0.6
$\Delta\theta_p$	0.0
$\Delta\varphi_p$	1.0
$\Delta\psi_p$	0.3

measurement and the intrinsic accuracy of the interpolation play a role in the overall observed accuracy. In fact, as discussed in the previous section, the casual errors in the data are too small to have an influence on the final result. On the other hand the systematic errors, known to arise both from small imperfection in the magnetic circuitry and from the finite resolution in the alignment of the measurement device, could be more relevant and need to be carefully studied. In particular, in Table 3 the Euler angles, representing the deviation of the measured field from the axial symmetry of the quadrupole, are listed from Ref. [9]. There the $\Delta\theta$, $\Delta\varphi$, $\Delta\psi$ parameters were connected to the magnetic circuit imperfections while the $\Delta\theta_p$, $\Delta\varphi_p$, $\Delta\psi_p$ were found as mainly due to the misplacement of the measurement probe.

The results are reasonably good for the B_y and B_z components for which a m.a.e. $\sim 0.15\%$ is obtained. These values are in fact compatible with the intrinsic accuracy of the interpolation since this is about 0.05 and 0.15% for these components. A different behaviour is found for the B_x , whose m.a.e. is about 0.35%, which is compatible with the systematic error of about 0.3% in this component. This is a little too large for the purpose of the direct application of trajectory reconstruction algorithms. If the source of such deviation is the systematic error in the measured data, a proper transformation of the field components and coordinates of the measurement points could compensate it and consequently improve the accuracy of the reconstructed field. Ideally such a transformation of the measured data generates the distribution that would have been obtained if the errors listed in Table 3 were null. Special attention needs to be paid to this point, as the two main sources of systematic error, i.e. the imperfection on magnetic circuitry and the systematic misplacement of the probe, have a different impact on the final achievable accuracy in the IMCM model. Both result in deviations of the measured magnetic field from the natural axial symmetry of the lens, which cannot be described by the technique discussed above since the image charge distribution is, by construction, axially symmetric. On the other hand, while the effects of the probe misplacement can be

reconstructed, providing that the rotation parameters are known, those due to the magnetic circuit should not be compensated, since they determine the actual shape of the magnetic field of the lens crossed by the particle trajectories. In that case, a possibility is to model the full magnetic field by an enlarged four-fold charge distribution, thus renouncing the symmetry condition, with the consequence of increasing considerably the complexity of the problem. Test calculations have shown that at the price of increasing the calculation time by almost two orders of magnitude, the overall accuracy is not significantly improved, mainly because of the effects of error propagation.

To account for the observed finite values of the $\Delta\theta_p$, $\Delta\varphi_p$, $\Delta\psi_p$ angles calculations were performed by applying the inverse rotation to the experimental data. Fig. 4 shows the ΔB_x distribution on the plane D obtained with the IMCM before and after this error compensation. As may be seen, the maximum deviation has been reduced. Also the m.a.e. and the m.s.e benefit from this coordinates correction by about a factor two, dropping down to values below 0.2%, which is slightly above the limit of the intrinsic accuracy of the interpolation technique. The residual part is likely due to the remaining contribution to the symmetry violation from the imperfection in the magnet circuit, which was not treated by the choice of a symmetric image charge distribution in the field model. This means that the interpolation method presented effectively compensates the systematic errors introduced by the experimental measurements, providing that the sources of those systematic errors on the data are sufficiently well known to allow the disentanglement of pure distortions of the field symmetries from spurious effects connected with the measurement instruments.

6. Conclusions

A method to reconstruct the three-dimensional field of a large quadrupole magnet has been presented. It is based on a superposition of fields generated by image charges with Gaussian distribution whose strengths are calculated by solving a best-fit problem based on the measured data. The resulting field is Maxwellian and infinitely differentiable, thus allowing the application of DA-techniques for the high order calculations of the ions trajectory through the MAGNEX spectrometer. Moreover, no extrapolation of the data from the medium plane is needed to determine the field in the whole space. This avoids high order differentiation, a process that could seriously disturb the focal plane image of the spectrometer.

The shape of the surface containing the centre of the charges has been found to be crucial to reduce the number of strengths to

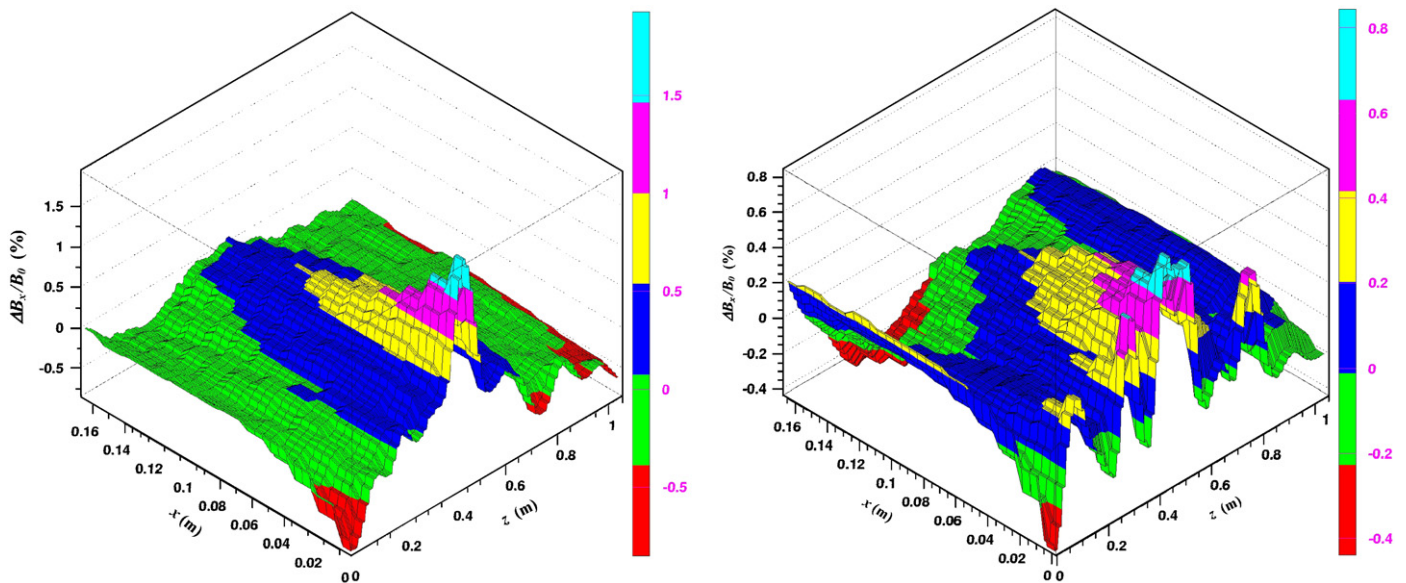


Fig. 4. ΔB_x distributions before (left) and after (right) compensation of systematic errors.

be calculated. This brings the computational effort to a tolerable limit such that time challenging procedures of optimization can be exploited. The LU-factorization method was the best choice for treatment of large matrices. In this way the parameters defining the geometry of the grid surface have been set up and the overall field reconstruction accuracy sensibly improved.

It was also shown that the method is sufficiently stable against both random and systematic source of errors to allow the application of the obtained field model to the challenging requirements of modern techniques of trajectory reconstruction. In particular the maximum admissible random noise is about $(\Delta B/B_0)_{max} = 3\%$ which is well beyond the 0.2% noise contained in the MAGNEX quadrupole data [9]. As regards the systematic error we found that an upper limit of about $(\Delta B/B_0)_{max} = 0.3\%$ is admissible to obtain a field accuracy compatible with the application of trajectory reconstruction. More specifically the accuracy of the B_y and B_z components lies below such limit, while it is above for the B_x as the m.a.e and m.s.e. are about 0.35% and 0.6%, respectively. In order to improve the overall accuracy, particularly that for the B_x component, a careful analysis of the main sources of the systematic error was performed, based on the control of the quadrupole four-fold symmetry [9]. In this way it became possible to partly remove such errors and consequently achieve the required accuracy for all the three reconstructed components of the field.

In conclusion we feel that the IMCM is a ground-breaking method that truly opens up the possibility of using 3D field measurements. In view of these results it has been applied to model the field both for the quadrupole and dipole lens of the

MAGNEX spectrometer. The details of the application of the IMCM to the MAGNEX dipole will be published in a forthcoming article.

References

- [1] M. Berz, LANL Technical Report AT-6: ATN-86-16, 1986.
- [2] M. Berz, K. Joh, J.A. Nolen, B.M. Sherrill, A.F. Zeller, Phys. Rev. C 47 (1993) 537.
- [3] A. Cunsolo, et al., in: Proceedings of the Giornata EXCYT, LNS Catania, January 16th 1996; A. Cunsolo, The MAGNEX Collaboration, Project MAGNEX proposal, INFN-LNS, Catania, 1996.
- [4] A. Cunsolo, F. Cappuzzello, A. Foti, A. Lazzaro, A.L. Melita, C. Nociforo, V. Shchepunov, J.S. Winfield, Nucl. Instr. and Meth. A 481 (2002) 48.
- [5] A. Cunsolo, F. Cappuzzello, A. Foti, A. Lazzaro, A.L. Melita, C. Nociforo, V. Shchepunov, J.S. Winfield, Nucl. Instr. and Meth. A 484 (2002) 56.
- [6] A. Lazzaro, The large acceptance and high resolution ray-tracing magnetic spectrometer MAGNEX, Ph.D. Thesis, University of Catania, 2002.
- [7] A. Lazzaro, F. Cappuzzello, A. Cunsolo, M. Cavallaro, A. Foti, A. Khouaja, S.E.A. Orrigo, J.S. Winfield, Nucl. Instr. and Meth. A 570 (2007) 192.
- [8] A. Lazzaro, F. Cappuzzello, A. Cunsolo, M. Cavallaro, A. Foti, S.E.A. Orrigo, M.R.D. Rodrigues, J.S. Winfield, Nucl. Instr. and Meth. A 585 (2008) 136.
- [9] A. Lazzaro, F. Cappuzzello, A. Cunsolo, M. Cavallaro, A. Foti, S.E.A. Orrigo, M.R.D. Rodrigues, J.S. Winfield, Nucl. Instr. and Meth. A 591 (2008) 394.
- [10] M. Berz, Modern Map Methods in Particle Beam Physics, Academic Press, ISBN 0-12-014750-5, 1999.
- [11] T. Mulvey, M.J. Wallington, Rep. Prog. Phys. 36 (1973) 347.
- [12] R. Degenhardt, M. Berz, Nucl. Instr. and Meth. A 427, in: Proceedings of CPO5, 1999, p. 151.
- [13] M. Berz, Nucl. Instr. and Meth. A 298 (1990) 426.
- [14] M. Berz, IEEE Trans. Electron Devices ED-35 (1988) 2002.
- [15] M. Berz, AIP Conf. Proc. 249 (1991) 456.
- [16] W.H. Press, S.A. Teukolsky, W.T. Vetterling, B.P. Flannery, second ed, Numerical Recipes in FORTRAN 77: The Art of Scientific Computing, vol. 1, Cambridge University Press, 1992.